Growth, electrical rectification, and gate control in axial *in situ* doped p-n junction germanium nanowires

Son T. Le,[1,a)] P. Jannaty,[1] A. Zaslavsky,[1] S. A. Dayeh,[2] and S. T. Picraux[2]
[1]*Department of Physics, Division of Engineering, Brown University, Providence, Rhode Island 02912, USA*
[2]*Center for Integrated Nanotechnologies, Los Alamos National Laboratory, Los Alamos, New Mexico 87545, USA*

(Received 13 May 2010; accepted 7 June 2010; published online 28 June 2010)

We report on vapor-liquid-solid growth and electrical properties of axial *in situ* doped p-n junction Ge sub-100 nm diameter nanowires. Room temperature four-point measurements show current rectification of two to three orders of magnitude depending on nanowire doping and diameter. We observe strong backgate control of reverse-bias current of up to three orders of magnitude and explain it by band-to-band tunneling modulated by the backgate-controlled electric field, as confirmed qualitatively via a quasi-three-dimensional Schrödinger–Poisson simulation. © *2010 American Institute of Physics*. [doi:10.1063/1.3457862]

Metal-catalyzed vapor-liquid-solid (VLS) growth of Si and Ge nanowires (NWs) is of great interest because of its possible compatibility with complementary metal-oxide-semiconductor technology.[1–3] Germanium devices are potentially attractive due to the higher carrier mobility and a better match between electron and hole mobilities compared to Si.[4–6] Controlled doping of Ge NWs, particularly in axial direction, is crucial for device applications. Several groups have demonstrated growth and electrical characterization of n-type or p-type[7] and p-n junction Ge NWs either by using sidewall doping (core-shell junctions)[8] or by growing p (n) Ge NWs on n^+ (p^+) Ge substrates to create NW-substrate junctions.[9] However, dopant incorporation through the NW surface[10] complicates the realization of axial p-n junction Ge NWs.

In this paper, we demonstrate axial *in situ* doped p-n junction Ge NWs of different diameters, D, and doping ratios that exhibit clear current rectification: the forward to reverse current ratio varies between 10^2 and 10^3. The ideality factor of the forward-bias current, obtained via four-point measurements on devices with Ohmic contacts, points to strong recombination in the NW depletion region and at the NW surface. In reverse bias, we observe effective backgate control of the current, which changes by three orders of magnitude as backgate voltage, V_{BG}, is scanned between 20 and −20 V. We attribute this to band-to-band tunneling (BTBT) modulation by the maximum junction field E_{MAX}, making our NWs equivalent to tunneling field effect transistors (TFETs) (Ref. 11) without an undoped region between the contacts.[12] We confirm this qualitatively via a quasi-three-dimensional (3D) Schrödinger–Poisson simulation in a simplified double-gate geometry.

The Ge NW p-n junctions were grown in a low pressure chemical vapor deposition reactor on Ge (111) surfaces with 20 and 50 nm Au colloids dispersed atop. We utilized GeH_4 (30% in H_2) as the source gas, and B_2H_6 and PH_3 (both at 100 ppm in H_2) as p- and n-type dopants, respectively. The growth procedure consisted of a two-step process[13] with ~1.5 min nucleation at ~360 °C followed by a 3 min temperature ramp down to ~280 °C where elongation of the p-n junction took place. GeH_4 flow was maintained throughout the growth of p-segment and n-segment with a constant chamber pressure of 2 Torr. The growth time was calibrated to produce a 2.8 μm long p-segment (slightly tapered in the presence of B_2H_6) (Ref. 14) followed by a 2.8 μm long n-segment. Figure 1(a) shows the thermal timeline of the growth process. For the VLS process to resume after a 30 s purge between p- and n-segment growth, the Au–Ge alloy

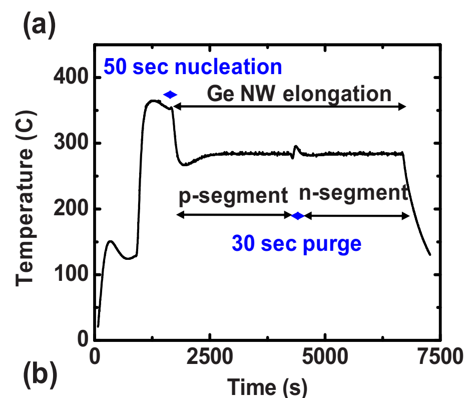

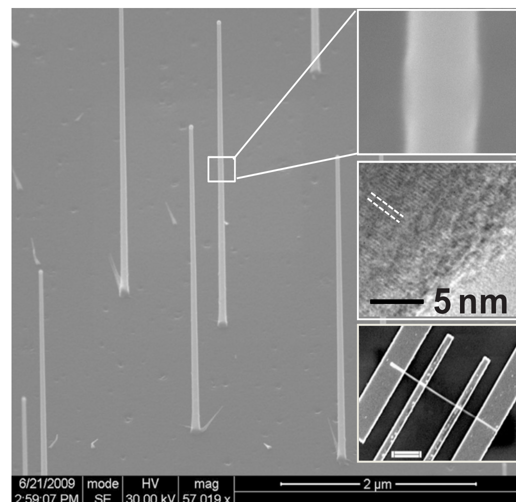

FIG. 1. (Color online) Growth and fabrication of p-n junction Ge NWs: (a) growth timeline; (b) SEM image, insets show junction position by SEM (top) and high-resolution TEM (middle), the bottom inset shows four-point device geometry with sputtered Ni contacts (scale bar is 1 μm).

a)Electronic mail: son_le@brown.edu.

 © 2010 American Institute of Physics

Downloaded 05 Jul 2010 to 192.12.184.2. Redistribution subject to AIP license or copyright; see http://apl.aip.org/apl/copyright.jsp

has to supersaturate in Ge leading to an increase in alloy diameter prior to resuming layer-by-layer Ge growth, resulting in a slight D increase at the p-n junction, as illustrated in Fig. 1(b) and its insets. These growth conditions allow optimal NW morphology for both the p-segment and n-segment without a significant shell overgrowth.[15]

It has been shown recently[6] that depletion width and hence the electrical characteristics of sub-100 nm NWs depend not only on the doping but also the diameter D due to fringing fields. Hence, we grew three different sets of NWs. For sample A growth, shown in Fig. 1(a), 40 nm Au colloids were used, with equal B_2H_6/GeH_4 and PH_3/GeH_4 molar fractions of 4.0×10^{-4}, resulting in nominal doping of 1×10^{19} cm^{-3} for the p-side and 4×10^{18} cm^{-3} for the n-side. Due to slight tapering of the wires during growth, the actual D was $\sim$60 nm at the junction position, see Fig. 1(b). Samples B and C runs used 50 nm and 20 nm Au colloids, respectively, and the nominal doping was reduced by a factor of 10 for the p-side and 4 for the n-side. To assist in the nucleation of the n-segment, the 30 s purge was eliminated for samples B and C. The resulting effective diameters at the junction were $D\sim75$ nm (growth B) and $D\sim30$ nm (growth C).

After growth, the NWs were suspended ultrasonically in an isopropanol solution and spread on a 450 nm thermal oxide covered n-Si wafer. The NW contacts were fabricated by e-beam lithography, $\sim$100 nm Ni sputter deposition and lift-off. After a dilute hydrofluoric acid dip, the samples were then covered by $\sim$150 nm of silicon dioxide deposited at 250 °C and annealed at 300 °C in forming gas for 15 min to improve the contacts via NiGe formation. An inset in Fig. 1(b) shows a top view scanning electron microscopy (SEM) image of the four-point device geometry after Ni contact lift-off. We performed energy dispersive spectroscopy (EDS) analysis (on a different test sample) along the NW after Ni contact formation to find that the NiGe extends $\sim$120 nm beyond the contact metal. This lateral diffusion of NiGe was taken into account in extracting the NW doping estimates.

It is known that Ni and NiGe make Ohmic contacts to p-Ge and Schottky contacts to n-Ge ($\varphi_{Bn}=0.74$ eV).[16,17] Our high doping density, however, leads to a thin tunneling barrier for the n-type Ge and results in a linear current-voltage characteristics away from the junction, shown in the inset of Fig. 2 for sample A. When measured across the p-n junction, all three NW devices show clear rectification. The ratio of forward to reverse current at $T=300$ K ranges from $\sim10^2$ (samples A and B) to $\sim10^3$ (sample C). Fitting the $I(V_D)$ characteristic with an ideal diode model:

$$I_D = I_0(e^{qV_D/nkT} - 1), \quad (1)$$

we obtained an ideality factor $n\sim2$ (samples A and B) and $n\sim2.3$ (sample C), as shown in Fig. 2. This suggests that, in forward bias, current is dominated by recombination,[17] as also recently observed in core-shell p-n junction Ge NWs.[8]

The Ohmic contact characteristics in the inset of Fig. 2 permit a doping estimate. Assuming the contact resistances on each (p or n) section of the wire to be the same, bulk Ge mobility, the NiGe formation from EDS measurements, and a surface state density[18] of 5×10^{12} cm^{-2}, we obtain the sample A p-doping level to be $\sim3.5\times10^{19}$ cm^{-3} and the n-doping level in the mid-10^{18} cm^{-3} range (the relatively close spacing of the n-section contacts make the n-section

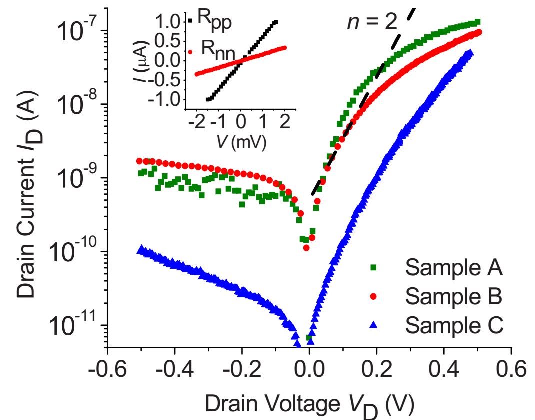

FIG. 2. (Color online) Current-voltage characteristics at $T=300$ K of *in situ* doped p-n junction Ge NWs showing rectification of up to three orders of magnitude (ideality factor $n=2$ is superimposed as guide to the eye). Inset shows the linear behavior of the p-segment and n-segment away from the junction (sample A), confirming low-resistance Ohmic contacts.

estimate less certain but it agrees with the nominal $\sim4\times10^{18}$ cm^{-3} doping expected from the growth parameters). Similar estimates on samples B and C, assuming the same 5×10^{12} cm^{-2} surface state density, confirm their doping to be $\sim2\times10^{18}$ range for p-side and $\sim1\times10^{18}$ for the n-side.

Figure 3 shows backgate control of $I(V_D, V_{BG})$ under reverse bias for constant V_{BG} values between -10 and 10 V, in 5 V steps for a different device from sample C ($D\sim30$ nm). After a rapid initial rise the reverse-bias I_D increases slowly with V_D, whereas V_{BG} exerts strong control over I_D (two orders of magnitude change between $V_{BG}=-10$ and 10 V). Positive V_{BG} increases I_D, consistent with the expected behavior where the lightly-doped side of the p-n junction controls the current. The inset in Fig. 3(a) shows $I(V_{BG})$ at constant reverse voltage $V_D=-0.5$ V and V_{BG} scanned between -20 and 20 V. The change in I_D is $\sim10^3$, corresponding to a large transconductance given that the backgate oxide is 450 nm thick. The $I(V_{BG})$ curve shows hysteresis consistent with a large surface state density at the $Ge-SiO_2$ interface.[18–21]

We attribute the gate control of the reverse-bias I_D to backgate-modulated BTBT. As described elsewhere,[17,22,23] the BTBT current follows an exponential dependence on E_{MAX} in the junction. However, an experimentally calibrated

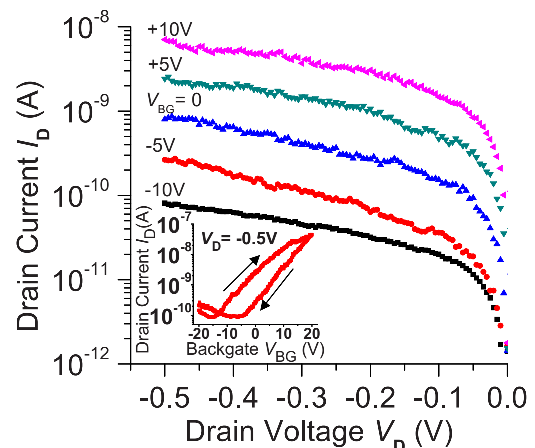

FIG. 3. (Color online) Dependence of reverse-bias I (sample C) on backgate voltage V_{BG}. Main panel shows $I(V_D)$ for different V_{BG}, inset shows $I(V_{BG})$ for constant $V_D=-0.5$ V, arrows indicate V_{BG} sweep direction.

Downloaded 05 Jul 2010 to 192.12.184.2. Redistribution subject to AIP license or copyright; see http://apl.aip.org/apl/copyright.jsp

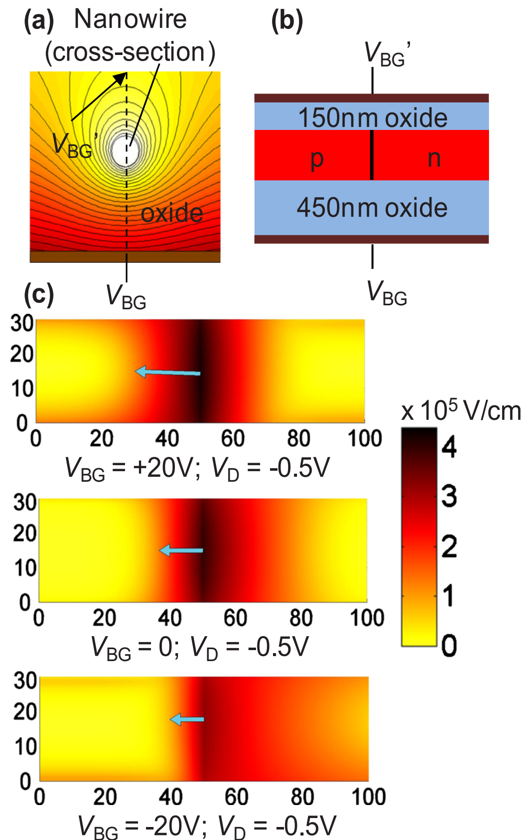

FIG. 4. (Color online) (a) Schematic NW geometry with potential field lines at $V_{BG}=+20$ V away from the junction; (b) simplified 2D double-gate model used to find the electric field; (c) electric field vs distance (nanometer) for $V_{BG}=+20$, 0, and -20 V, with $V_D=-0.5$ V, where arrows indicate position, direction, and magnitude of E_{MAX}.

analytical expression for BTBT in Ge is not available and contains unknown factors,[24,25] especially since E_{MAX} need not align with the NW axis or a definite crystallographic direction. As a result, we will restrict our analysis to estimating the E_{MAX} in our Ge NWs as a function of V_{BG}.

A full evaluation of E_{MAX} in our NWs would require a fairly complex 3D Schrödinger–Poisson solution as shown in Fig. 4(a). Simpler qualitative insight into the V_{BG} control of E_{MAX} and hence of BTBT-dominated I_D can be obtained using a simplified two-dimensional (2D) double-gate geometry of Fig. 4(b), where V_{BG} is applied to the bottom gate and a smaller V'_{BG} to the top gate. The justification for choosing the double-gate geometry came from our Poisson solution of potential distribution for the oxide-covered NW geometry away from the junction, see Fig. 4(a). We found that due to the fringing fields, the potential V'_{BG} at the top of the passivation oxide is smaller than V_{BG} but not negligible: for example, for $V_{BG}=20$ V, $V'_{BG}\sim 4.7$ V. We then applied V'_{BG} to the top gate of the double-gate geometry shown in Fig. 4(b). The channel height in Fig. 4(b) was taken as $D\sim 30$ nm, doping values were 2×10^{18} cm^{-3} (p-side) and 10^{18} cm^{-3} (n-side) consistent with our doping estimates, and the distance between the NW and the bottom (top) gate was 450 (150) nm, corresponding to the actual oxide thicknesses. The axial length was taken to be 100 nm, with the p-n junction located at the midpoint and assumed to be ideally abrupt.

Figure 4(c) shows Schrödinger–Poisson solutions of E_{MAX} at $V_D=-0.5$ V and $V_{BG}=20$, 0, and -20 V. The simulated E_{MAX} at $V_{BG}=20$ V is much higher ($\sim$double) than at $V_{BG}=-20$ V, in qualitative agreement with the observed strong backgate control of I_D. Clearly, full 3D modeling would be necessary to obtain E_{MAX} quantitatively. An additional complication is that while our model assumed uniform doping in the p and n regions, measurements on VLS-grown *in situ* doped NWs indicate higher doping (and hence higher field) closer to the outside of the NW.[26]

In conclusion, we have demonstrated the growth and electrical properties of *in situ* doped axial p-n junction Ge NWs for diameters ranging from 30 to 75 nm. Fabricated devices show current rectification with forward/reverse current ratio of up to three orders of magnitude, as well as strong backgate control of the NW reverse-bias current that we attribute to high-field BTBT.

The work at Brown was supported by the NSF (Award No. ECCS-0701635) and at Los Alamos National Laboratory by the Laboratory Directed Research and Development Program. Work was performed, in part, at the Center for Integrated Nanotechnologies, a U.S. Department of Energy, Office of Basic Energy Sciences user facility.

[1]Y. Cui, Z. H. Zong, D. L. Wang, W. U. Wang, and C. M. Lieber, Nano Lett. **3**, 149 (2003).
[2]S. Hoffmann, J. Bauer, C. Ronning, Th. Stelzner, J. Michler, C. Ballif, V. Sivakov, and S. H. Christiansen, Nano Lett. **9**, 1341 (2009).
[3]J. G. Swadener and S. T. Picraux, J. Appl. Phys. **105**, 044310 (2009).
[4]J. Xiang, W. Lu, Y. J. Hu, H. Yan, and C. M. Lieber, Nature (London) **441**, 489 (2006).
[5]T. Shimizu, Z. Zhang, S. Shingubara, S. Senz, and U. Gosele, Nano Lett. **9**, 1523 (2009).
[6]F. Léonard, A. A. Talin, B. S. Swartzentruber, and S. T. Picraux, Phys. Rev. Lett. **102**, 106805 (2009).
[7]A. B. Greytak, L. J. Lauhon, M. S. Gudiksen, and C. M. Lieber, Appl. Phys. Lett. **84**, 4176 (2004).
[8]E. Tutuc, J. Appenzeller, M. C. Reuter, and S. Guha, Nano Lett. **6**, 2070 (2006).
[9]P. W. Leu, H. Adhikari, M. Koto, K. H. Kim, P. Rouffignac, A. F. Marshall, R. G. Gordon, C. E. D. Chidsey, and P. C. McIntyre, Nanotechnology **19**, 485705 (2008).
[10]E. Tutuc, J. O. Chu, J. A. Ott, and S. Guha, Appl. Phys. Lett. **89**, 263101 (2006).
[11]M. T. Björk, J. Knoch, H. Schmid, H. Riel, and W. Riess, Appl. Phys. Lett. **92**, 193504 (2008).
[12]C. Aydin, A. Zaslavsky, S. Luryi, S. Cristoloveanu, D. Mariolle, D. Fraboulet, and S. Deleonibus, Appl. Phys. Lett. **84**, 1780 (2004).
[13]D. Wang, Q. Wang, A. Javey, R. Tu, H. Dai, H. Kim, P. C. McIntyre, T. Krishnamohan, and K. C. Saraswat, Appl. Phys. Lett. **83**, 2432 (2003).
[14]E. Tutuc, S. Guha, and J. O. Chu, Appl. Phys. Lett. **88**, 043113 (2006).
[15]S. A. Dayeh and S. T. Picraux, "Direct observation of nanoscale size effects in Ge semiconductor nanowire growth," Nano Lett. (to be published).
[16]R. Li, H. B. Yao, S. J. Lee, D. Z. Chi, M. B. Yu, G. Q. Lo, and D. L. Kwong, Thin Solid Films **504**, 28 (2006).
[17]S. M. Sze, *Physics of Semiconductor Devices*, 2nd ed. (Wiley, New York, 1981).
[18]S. X. Zhang, E. R. Hemesath, D. E. Perea, E. Wijaya, J. L. Lensch-Falk, and L. J. Lauhon, Nano Lett. **9**, 3268 (2009).
[19]T. Hanrath and B. A. Korgel, J. Phys. Chem. B **109**, 5518 (2005).
[20]A. Dimoulas and P. Tsipas, Microelectron. Eng. **86**, 1577 (2009).
[21]D. Wang, Y. L. Chang, Q. Wang, J. Cao, D. B. Famer, R. G. Gordon, and H. Dai, J. Am. Chem. Soc. **126**, 11602 (2004).
[22]E. O. Kane, J. Phys. Chem. Solids **12**, 181 (1960).
[23]P. M. Solomon, J. Jopling, D. J. Frank, C. D'Emic, O. Dokumaci, P. Ronsheim, and W. E. Haensch, J. Appl. Phys. **95**, 5800 (2004).
[24]S. O. Koswatta, M. S. Lundstrom, and D. E. Nikonov, Appl. Phys. Lett. **92**, 043125 (2008).
[25]C. Rivas, R. Lake, G. Klimeck, W. R. Frensley, M. V. Fischetti, P. E. Thompson, S. L. Rommel, and P. R. Berger, Appl. Phys. Lett. **78**, 814 (2001).
[26]D. E. Perea, E. R. Hemesath, E. J. Schwalbach, J. L. Lensch-Falk, P. W. Voorhees, and L. J. Lauhon, Nat. Nanotechnol. **4**, 315 (2009).

Downloaded 05 Jul 2010 to 192.12.184.2. Redistribution subject to AIP license or copyright; see http://apl.aip.org/apl/copyright.jsp